Calibration methods influence quantitative material decomposition in photon-counting spectral CT

Tyler E. Curtis and Ryan K. Roeder*

Department of Aerospace and Mechanical Engineering, Bioengineering Graduate Program, University of Notre Dame, Notre Dame, IN 46556, USA

ABSTRACT

Photon-counting detectors and nanoparticle contrast agents can potentially enable molecular imaging and material decomposition in computed tomography (CT). Material decomposition has been investigated using both simulated and acquired data sets. However, the effect of calibration methods on material decomposition has not been systematically investigated. Therefore, the objective of this study was to investigate the influence of the range and number of contrast agent concentrations within a modular calibration phantom on quantitative material decomposition. A commercially-available photon-counting spectral micro-CT (MARS Bioimaging) was used to acquire images with five energy bins selected to normalize photon counts and leverage the contrast agent *k*-edge. Material basis matrix values were determined using multiple linear regression models and material decomposition was performed using a maximum *a posteriori* estimator. The accuracy of quantitative material decomposition was evaluated by the root mean squared error (RMSE), specificity, sensitivity, and area under the curve (AUC). An increased maximum concentration (range) in the calibration significantly improved RMSE, specificity and AUC. The effects of an increased number of concentrations in the calibration were not statistically significant for the conditions in this study. The overall results demonstrated that the accuracy of quantitative material decomposition in spectral CT is significantly influenced by calibration methods, which must therefore be carefully considered for the intended diagnostic imaging application.

Keywords: Calibration phantom, contrast media, material decomposition, photon counting detector, spectral computed tomography

1. PURPOSE

X-ray computed tomography (CT) provides low cost anatomic and diagnostic imaging at high spatial and temporal resolution.[1-3] Conventional clinical and laboratory CT imaging systems utilize a polychromatic X-ray source with a photon energy spectrum ranging from a lower threshold of ~20 keV, set by beam filtration, to a peak tube potential of 80-140 kVp.[3] Materials and tissues exhibit photon energy-dependent differences in X-ray attenuation coefficients over this energy range.[4,5] However, conventional CT systems utilize an energy integrating detector, which sums the photon counts over the entire energy spectrum, ignoring energy-specific spectral information.[6] Dual-energy CT (DECT) captures limited energy-dependent differences by imaging at two peak tube potentials and applying a weighted subtraction to decompose and quantify material composition.[7,8] However, DECT increases radiation exposure and is typically limited to the separation of two materials, usually soft tissue and high attenuators, such as bone or contrast media.[7,8] Multi-energy acquisition is required to decompose a greater number of material and tissue compositions.

Recent advances in energy-sensitive X-ray detectors have enabled multi-energy or spectral CT using a single polychromatic X-ray source.[9,10] Energy-sensitive detectors measure the number of photon interactions with the detector and the energy of each interaction by the charge output of the detector chip. Advances in photon-counting detectors (PCDs) have decreased the computational time required to evaluate these interactions, allowing photon energies to be accurately measured in high flux, multi-pixel applications. PCDs, such as the Medipix 3RX, make count corrections for charge summing and pulse pileup, based upon the pulse height and analysis of coinciding detector interactions, decreasing spectral blurring and increasing image quality.[9,11,12] The measured energy-dependent attenuation coefficients enable identification of material composition (material decomposition).[13-17] Material decomposition has been investigated with photon-counting CT using both simulated[14,15,18] and acquired data sets.[13,18,19] These investigations have primarily focused on algorithm design. However, the effect of calibration methods on quantitative material decomposition has not been experimentally investigated.

* rroeder@nd.edu; phone 1-574-631-7003; https://engineering.nd.edu/profiles/rroeder

Medical Imaging 2017: Physics of Medical Imaging, edited by Thomas G. Flohr, Joseph Y. Lo, Taly Gilat Schmidt, Proc. of SPIE Vol. 10132, 101323L · © 2017 SPIE
CCC code: 1605-7422/17/$18 · doi: 10.1117/12.2255661

Therefore, the purpose of this study was to investigate the influence of the range and number of contrast agent concentrations within a modular calibration phantom on material decomposition. A systematic analysis of calibration phantom concentrations was performed using a commercially-available photon-counting spectral micro-CT system with five energy bins selected to normalize photon counts and leverage the contrast agent *k*-edge. An increase in the maximum concentration (range) and number of concentrations utilized in the calibration was hypothesized to result in an increased signal-to-noise ratio in each energy bin for improved accuracy and precision of quantitative material decomposition.

2. MATERIALS AND METHODS

2.1. Calibration phantom

Gadolinium was chosen as a model contrast agent for spectral CT due to clinical use as a contrast agent for diagnostic imaging and the presence of a *k*-shell absorption edge within the clinical X-ray energy spectrum. Gadolinium nitrate, $Gd(NO_3)_3 \cdot 6H_2O$ (Acros Organics, 99.9%), solutions were prepared in deionized (DI) water at selected concentrations ranging from 0 to 90 mM. The maximum gadolinium concentration (30, 60, and 90 mM) and total number of gadolinium concentrations (2, 4, and 7) were independently varied to investigate the effect on quantitative material decomposition (Table 1). Calcium signal was calibrated using a custom bone mineral density phantom with compositions ranging from 0 to 60 vol% (0-1860 mg/cm^3) hydroxyapatite in polyethylene.[20]

Table 1. The range and number of gadolinium contrast agent concentrations used to systematically investigate the effect of calibration methods on quantitative material decomposition.

Concentration Range	Maximum Concentration (mM)	Number of Concentrations	Step Size (mM)
30 x 2	30	2	30
30 x 4	30	4	10
30 x 7	30	7	5
60 x 4	60	4	20
90 x 4	90	4	30

Gadolinium concentrations were verified by inductively coupled plasma optical emission spectroscopy (ICP-OES, Optima 7000, Perkin Elmer) after digesting samples in 5% nitric acid. Calibration curves for ICP-OES were created by diluting certified standard gadolinium solutions (SPEX CertiPrep, assurance grade). Measured gadolinium concentrations were compared with the expected concentrations using linear least squares regression and a paired *t*-test (JMP® 11.0, SAS Institute).

2.2. Sample phantom

A sample phantom containing 0, 5, and 10 mM concentrations of gadolinium nitrate dissolved in DI water, as well as a rabbit femur embedded in 1% agarose (Thermo Scientific, molecular biology grade) was used to evaluate the material decomposition calibrations. The range of contrast agent concentrations was selected to be feasible for targeted delivery based upon pre-clinical animal models while challenging the detection limit of conventional CT.[21]

2.3. Image acquisition

For both the calibration and sample phantoms, Eppendorf tubes containing each gadolinium and calcium concentration were placed in a modular phantom for imaging. Images of both the calibration and sample phantoms, as well as flatfield correction images, were acquired using a commercially-available spectral CT (MARS Bioimaging, Christchurch, NZ) equipped with a polychromatic X-ray source operating at 120 kVp, 1.96 mm aluminum beam filtration, and a photon-counting detector (Medipix 3RX) with five energy bins. Energy thresholds were set at 30.9, 50.0, 60.1, and 73.1 keV to normalize photon counts across energy bins and leverage the *k*-edge discontinuity of gadolinium at 50.2 keV.[22] Reconstructions were performed with a 100 μm isometric voxel size and a nominal resolution of ~300 μm. Five replicates were imaged for each calibration range (Table 1). The phantom design and relatively low contrast agent concentrations obviated the need for beam hardening correction due to the absence of hard attenuators in-line with the X-ray source.

2.4. Basis matrix

The material basis matrix (C) is an M x N matrix of the calculated attenuation coefficients for each material in each energy bin, where M is the number of energy bins and N is the number of materials to be decomposed. Attenuation is assumed to be approximately linear for each composition on a bin by bin basis. The measured attenuation within a pixel after flatfield correction is described by,

$$-ln(I/I_o)=\sum_{i=1}^{N}(\mu_i x_i) \tag{1}$$

where I is the X-ray intensity at the detector, I_o is the source X-ray intensity, μ_i is the attenuation of the i-th material, x_i is the distance the X-ray beam travels through the i-th material, and N is the number of materials to be decomposed. The left side of Eq. (1) is equivalent to the measured attenuation after reconstruction. The attenuation coefficient of gadolinium in each energy bin was determined using a multiple linear regression of known gadolinium compositions as,

$$y=b_o+b_1x_1+b_2x_2 \tag{2}$$

where y is the observed linear X-ray attenuation, b_o is the intercept, which was assumed to be zero, b_1 is the attenuation coefficient of gadolinium, and b_2 is the attenuation coefficient of water. Given the known concentrations of gadolinium in each calibration range (Table 1), the theoretical volume fraction of gadolinium and water in each composition was estimated using,

$$v_1\approx\frac{(m_1/\rho_1)}{(m_1/\rho_1+m_2/\rho_2)} \tag{3}$$

where v_1 is the volume fraction of gadolinium, m_1 and m_2 are the mass of gadolinium and water respectively, ρ_1 and ρ_2 are the density of gadolinium and water, respectively, and the volume fraction of water is $v_2 \approx 1 - v_1$. The linear model was then computed using the estimated volume fraction of gadolinium and water, and the mean X-ray attenuation measured within a 97 mm^3 cuboidal volume of interest (VOI) for each calibration composition and replicate. The calculation was repeated for each of the five energy bins to complete the basis matrix. The estimated X-ray attenuation coefficients of gadolinium and water were paired for each calibration set and replicate. The same process was repeated for the calcium calibration phantom, using the volume fraction of hydroxyapatite and polyethylene as the input variables. A single vector of calcium attenuation coefficients was calculated and used for all material basis matrices.

2.4. Material decomposition

Material decomposition was performed using a quadratic programming function (quadprog, MATLAB, v. 9.0, MathWorks Inc.) with a maximum *a posteriori* (MAP) estimator[23] on the sample image using the basis matrices calculated for each calibration range. A MAP estimator was chosen to mitigate the large number of possible solutions to the linear system of equations, which were constrained to satisfy both full additivity and non-negativity constraints. The volume fraction of materials in each voxel of the sample image was estimated by minimizing the equation,

$$min_x\ 0.5\cdot x^T\cdot H\cdot x + f^T\cdot x \tag{4}$$

where x is a vector of volume fractions of length N, and

$$H = 2\cdot C^T\cdot C \tag{5}$$

$$f= -2\cdot C^T\cdot x \tag{6}$$

such that,

$$A\cdot x\le b \tag{7}$$

$$A_{eq}\cdot x = b_{eq} \tag{8}$$

$$A=\begin{bmatrix}1 & 0 & 0\\ 0 & \ddots & 0\\ 0 & 0 & 1_N\\ -1 & 0 & 0\\ 0 & \ddots & 0\\ 0 & 0 & -1_N\end{bmatrix} \tag{9}$$

where b is an N x 2 vector containing N ones and N zeros, A_{eq} is a vector of length N comprised of ones, and b_{eq} is equal to one. Eq. (7) limits the solution to remain between 0 and 1, satisfying the non-negativity constraint. Eq. (8) ensures that the vector of volume fractions sums to 1 for each voxel, satisfying the full additivity constraint.

2.5. Post-decomposition scaling

Post-decomposition scaling was utilized to quantify the material decomposition as material concentration. The mean X-ray attenuation of each concentration within the calibration VOI was determined for all energy bins. These mean attenuation values were then decomposed using the MAP estimator for each of the basis matrices used for material decomposition. The estimated volume fraction of each concentration was correlated with the known concentration (mM) in the calibration. Linear least squares regression was performed for each calibration phantom, using the same dataset for decomposition as scaling. The intercept, b_o, was allowed to be non-zero to determine the best-fit regression line. Decomposed images were then scaled to mM concentrations using linear regression.

2.6. Evaluation of quantitative material decomposition

Material decomposition of gadolinium, calcium, and water was performed on the sample image for each calibration method (Table 1). Evaluation of the effects of the calibration method on quantitative material decomposition was limited to the gadolinium concentration to focus on contrast media and simplify interpretation. True positive VOIs included the two concentrations of gadolinium; true negative VOIs included the water and rabbit bone. Each VOI was 101 mm^3 including 20 slices of the reconstruction within the inner diameter of each Eppendorf tube. The accuracy of the quantitative material decomposition for each calibration method was evaluated by measuring the root mean squared error (RMSE) of the measured gadolinium concentrations compared with the known concentrations within the sample phantom. The spatial accuracy of the quantitative material decomposition for each calibration method was evaluated by measuring the specificity and sensitivity at a 5 mM threshold. Area under the curve (AUC) was also calculated by evaluating the specificity and sensitivity over a range of concentrations (0 – 20 mM) which exceeded the concentrations within the sample phantom. The RMSE, specificity, sensitivity, and AUC for each calibration method were compared using box plots showing the 10th, 25th, 50th (median), 75th and 90th percentiles from five replicates. Effects of the range and number of contrast agent concentrations in the calibration phantom on RMSE, specificity, sensitivity, and AUC were examined using one-way analysis of variance (ANOVA), and *post-hoc* comparisons were performed using Mann-Whitney *U*-tests (JMP® 11.0, SAS Institute).

3. RESULTS

3.1. Calibration phantoms

The accuracy of gadolinium concentrations in the calibration phantom was verified by ICP-OES (Fig. 1). Measured gadolinium concentrations exhibited a strong linear correlation with the expected concentration ($p < 0.0001$, $R^2 = 0.999$). Overall, measured gadolinium concentrations were greater than the expected concentration ($p < 0.0001$ paired *t*-test) with a RMSE of 3.4 mM.

3.2. Maximum concentration (range)

The effect of the range of contrast agent concentrations in the calibration phantom was investigated by varying the maximum concentration within the calibration phantom (30, 60, and 90 mM) while maintaining a total of four concentrations equally distributed between zero and the maximum concentration (Table 1). Gadolinium segmented images of a representative sample phantom after material decomposition qualitatively demonstrated that overall image quality was visually improved when the maximum concentration in the calibration exceeded 30 mM (Fig. 1a). Specificity for gadolinium compared with hard attenuators was compromised using the lowest maximum concentration (30 mM) in the calibration as evidenced by the presence of gadolinium signal in the bone sample (Fig. 1a). On the other hand, specificity for gadolinium compared with soft attenuators (e.g., polypropylene sample tubes) not included in the basis matrix was improved using the lowest maximum concentration (30 mM) in the calibration (Fig. 1a). Quantitative evaluation of material decomposition revealed that calibration using a greater concentration range significantly improved the RMSE (Fig. 1b), specificity (Fig. 1d), and AUC (Fig. 1e) ($p < 0.005$, ANOVA). Sensitivity was significantly decreased with a greater concentration range (Fig. 1c) ($p < 0.05$, ANOVA). Importantly, the median RMSE was ~2.5 and ~1.2 mM for a

maximum calibration concentration of 30 and 90 mM, respectively, which is similar in magnitude to the RMSE measured by ICP-OES.

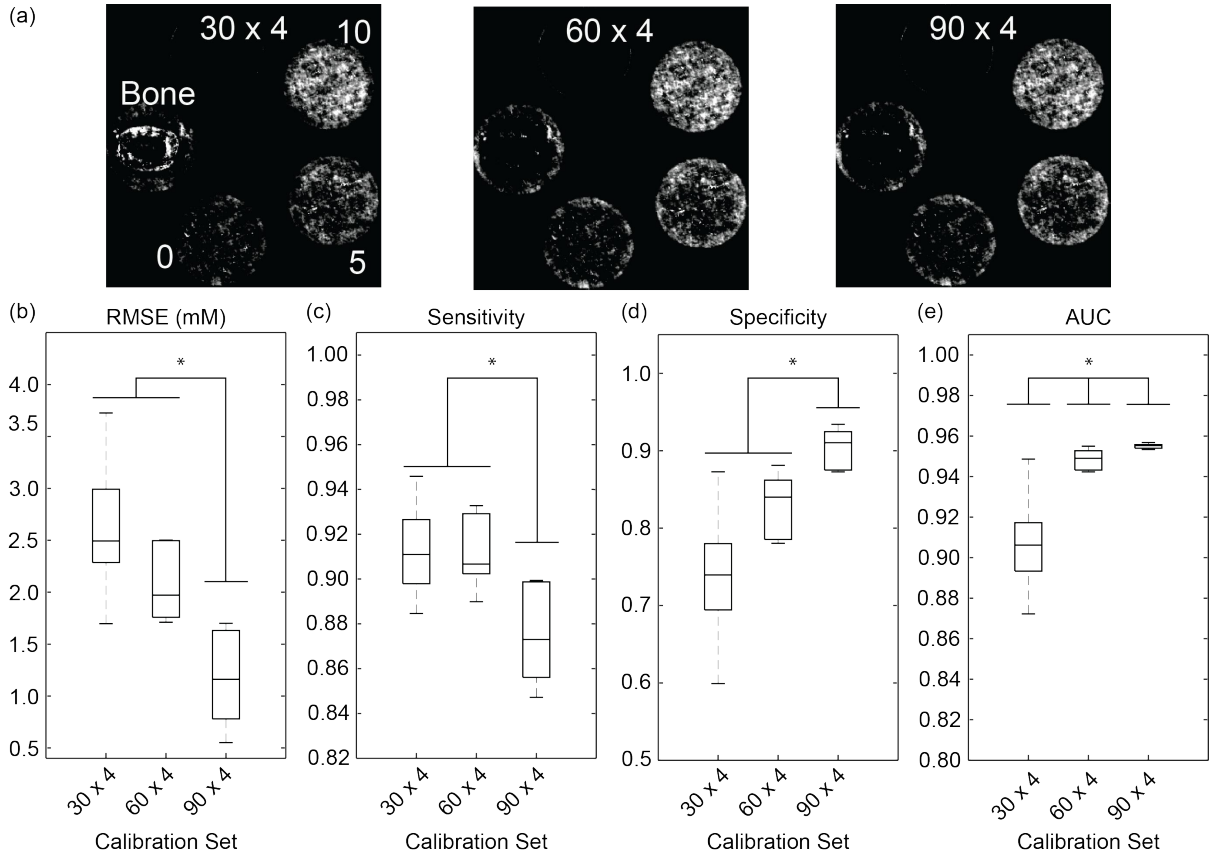

Figure 1. Effects of the range of contrast agent concentrations (30, 60, and 90 mM) in the calibration phantom with four total concentrations (Table 1) on quantitative material decomposition. (a) Representative gadolinium segmented images of the same sample phantom after gadolinium material decomposition using a minimum and maximum threshold for gadolinium segmentation of 0 and 20 mM, respectively. Boxplots showing the (b) RMSE, (c) sensitivity, (d) specificity, and (e) AUC of the resulting quantitative material decomposition for each calibration method. The box and whiskers show the 10th, 25th, 50th, 75th, and 90th percentiles. Asterisks show statistically significant difference between groups (Mann-Whitney *U*-test).

3.3. Number of concentrations

The effect of the number of contrast agent concentrations in the calibration phantom was investigated by varying the number of equally distributed concentrations within the calibration phantom (2, 4, and 7 concentrations) while maintaining a 30 mM maximum concentration (Table 1). Gadolinium segmented images of a representative sample phantom after material decomposition qualitatively demonstrated that specificity was visually improved with an increased number of concentrations (Fig. 2a) for both hard (e.g., bone) and soft (e.g., polypropylene sample tubes). Quantitative evaluation of material decomposition revealed that calibration using a greater number of concentrations did not significantly improve the RMSE (Fig. 2b), sensitivity (Fig. 2c), or specificity (Fig. 2d) ($p > 0.63$, ANOVA). AUC appeared to be improved with an increased number of concentrations (Fig. 2e), but the difference was smaller in magnitude compared with the effect of the maximum concentration was not statistically significant ($p > 0.09$, ANOVA).

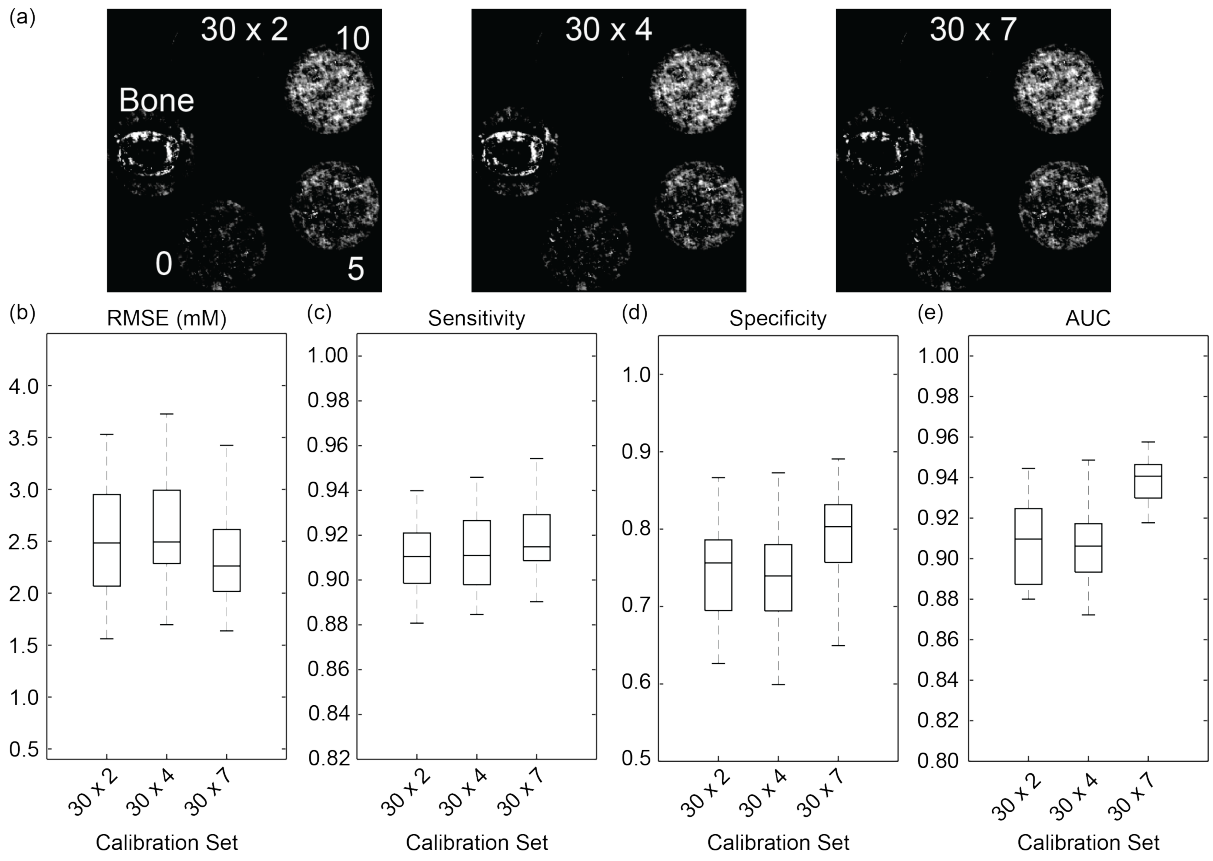

Figure 2. Effects of the number of contrast agent concentrations (2, 4, and 7 samples) in the calibration phantom with a maximum concentration of 30 mM (Table 1) on quantitative material decomposition. (a) Representative gadolinium segmented images of the same sample phantom after gadolinium material decomposition using a minimum and maximum threshold for gadolinium segmentation of 0 and 20 mM, respectively. Boxplots showing the (b) RMSE, (c) sensitivity, (d) specificity, and (e) AUC of the resulting quantitative material decomposition for each calibration method. The box and whiskers show the 10th, 25th, 50th, 75th, and 90th percentiles. Differences between groups were not statistically significant ($p > 0.09$, Mann-Whitney U-test)

4. DISCUSSION

The results of this study demonstrate important effects of calibration methods on quantitative material decomposition using photon-counting spectral CT. First, and most importantly, both the quantitative (RMSE) and spatial accuracy (AUC) of material decomposition was significantly improved using an increased maximum concentration (range) in the basis matrix calibration (Fig. 1). A small decrease in sensitivity with increased concentration range was greatly outweighed by improvements in specificity, as reflected in the measured AUC. AUC measures the relative gain in specificity with decreasing sensitivity over a range of thresholds and is therefore a robust metric of spatial accuracy. Therefore, the results of this study suggest that an increased contrast agent concentration range provided a greater signal-to-noise ratio during calibration, which subsequently improved the accuracy of quantitative material decomposition.

Secondly, in contrast to our hypothesis, a greater number of contrast agent concentrations did not produce a statistically significant improvement in either the quantitative (RMSE) or spatial accuracy (AUC) of material decomposition (Fig. 2). Increasing the number of concentrations (or samples) was expected to reduce variance in the linear regression models, improving the accuracy of the basis matrix values and the subsequent material decomposition. Retrospective power analysis revealed that the apparent increase in AUC with an increased number of concentrations would have been statistically significant with an increase in the sample size from 5 to 6 replicates per calibration method. Moreover, representative images appeared to show visual improvement in spatial accuracy with an increased number of concentrations in the calibration (Fig. 2a), but this improvement was subtle compared with that from an increased

maximum concentration (Fig. 1a). Nonetheless, the results of this study suggest that calibration methods for quantitative material decomposition may not require more than two concentrations of a material of interest for some applications, which could simplify the calibration methods and computational burden.

This study was not without limitations. The analysis quantitative and spatial accuracy only included the decomposition of gadolinium to simplify the interpretation of results. However, the hard-constrained MAP estimator requires a fully defined basis matrix to produce accurate results. Therefore, fluctuations within the vector of values used to define the gadolinium signal can adversely affect the results of other material channels. All material channels should be considered simultaneously in order to fully characterize a basis matrix calibration. Perhaps most importantly, this study did not consider the effects of the calibration method on the material basis matrix and scaling factor separately. All analyses used the same calibration method for both the material basis matrix and scaling factor rather than uncoupling these effects. Last, evaluation of the effect of the concentration range was limited to a total number of four concentrations, and the effect the number of concentrations was limited to a maximum concentration of 30 mM. To address these limitations, further investigation will include a greater number of combinations in the range and number of concentrations in the calibration, and will investigate effects on the material basis matrix and scaling factor separately.

5. CONCLUSIONS

Both the quantitative (RMSE) and spatial accuracy (AUC) of material decomposition in photon-counting spectral CT was significantly improved using an increased maximum concentration (range) in the calibration. On the other hand, an increased number of concentrations (or samples) did not produce a statistically significant improvement in either the quantitative (RMSE) or spatial accuracy (AUC) of material decomposition (Fig. 2) under the conditions of this study. The overall results demonstrated that quantitative material decomposition in spectral CT is significantly influenced by calibration methods and should be carefully considered for an intended diagnostic imaging application.

ACKNOWLEDGMENTS

This research was supported by grants from the National Science Foundation (DMR-1309587), Kelly Cares Foundation, St. Joseph Regional Medical Center, and the University of Notre Dame Equipment Renewal and Restoration Program. The authors also acknowledge MARS Bioimaging (Christchurch, NZ), the Notre Dame Integrated Imaging Facility (NDIIF), the Notre Dame Center for Environmental Science and Technology (CEST) for ICP-OES, and that some of the software used in this study was initially developed by T.E. Curtis at the Physiological Research Imaging Laboratory at the Mayo Clinic College of Medicine.

REFERENCES

[1] Kircher, M.F. and Willmann, J.K., "Molecular body imaging: MR imaging, CT, and US. Part I. Principles," Radiology 263(3), 633-643 (2012).
[2] Nam, S.Y., Ricles, L.M., Suggs, L.J. and Emelianov, S.Y, "Imaging strategies for tissue engineering applications," Tissue Eng. Part B Rev. 21(1), 88-102 (2014).
[3] Kalender, W.A., "X-Ray computed tomography," Phys. Med. Biol. 51(13), R29-R43 (2006).
[4] Hubbell, J.H. and Seltzer, S.M., "Table of X-ray mass attenuation coefficients and mass energy-absorption coefficients (version 1.4)," National Institute of Standards and Technology, Gaithersburg, MD (2004). Available at http://physics.nist.gov/xaamdi.
[5] Hubbell, J.H., Gimm, H.A. and Overbo, I., "Pair, triplet, and total atomic cross sections (and mass attenuation coefficients) for 1 MeV-100 GeV photons in elements Z = 1 to 100," J. Phys. Chem. Ref. Data 9, 1023-1148 (1980).
[6] He, P., Yu, H., Bennett, J., Ronaldson, P., Zainon, R., Butler, A., Butler, P., Wei, B. and Wang G., "Energy-discriminative performance of a spectral micro-CT system," J. X-Ray Sci. Technol. 21(3), 335-345 (2013).
[7] Graser, A., Johnson, T.R., Chandarana, H. and Macari, M., "Dual energy CT: preliminary observations and potential clinical applications in the abdomen," Eur. Radiol. 19(1), 13-23 (2009).
[8] Johnson, T.R.C., Kraub, B., Sedlmair, M., Grasruck, M., Bruder, H., Morhard, D., Fink, C., Weckbach, S., Lenhard, M., Schmidt, B., Flohr, T., Reiser, M.F. and Becker, C.R., "Material differentiation by dual energy CT: initial experience," Eur. Radiol. 17(6), 1510-1517 (2007).
[9] Roessl, E. and Proksa R., "K-edge imaging in X-ray computed tomography using multi-bin photon counting detectors," Phys. Med. Biol. 52(15), 4679-4696 (2007).

[10] Yu, Z., Leng, S.M., Jorgensen, S., Li, Z., Gutjahr, R., Chen, B., Duan, X., Halaweish, A., Yu, L. and Ritman, E.L., "Initial results from a prototype whole-body photon-counting computed tomography system," Proc. SPIE 9412, 94210W-94210W-7 (2015).
[11] Ballabriga, R., Campbell, M., Heijne, E., Llopart, X., Tlustos, L. and Wong, W., "Medipix3: A 64 k pixel detector readout chip working in single photon counting mode with improved spectrometric performance," Nucl. Instr. Meth. Phys. Res. A, **633**, S15-S18 (2011).
[12] Jorgensen, S.M., Vercnocke, A.J., Rundle, D.S., Butler, P.H., McCollough, C.H. and Ritman, E.L., "Evaluation of a photon counting Medipix3RX CZT spectral X-ray detector" Proc. SPIE 9969, 99690J-99690J-8 (2016).
[13] Alessio, A.M., and MacDonald, L.R., "Quantitative material characterization from multi-energy photon counting CT," Med. Phys. 40(3), 031108 (2013).
[14] Le, H.Q. and Molloi, S., "Least squares parameter estimation methods for material decomposition with energy discriminating detectors," Med. Phys. 38(1), 245-255 (2011).
[15] Barber, R.F., Sidky, E.Y., Schmidt, T.G. and Pan, X.C., "An algorithm for constrained one-step inversion of spectral CT data," Phys. Med. Biol. 61(10), 3784-3818 (2016).
[16] Weidinger, T., Buzug, T.M., Flohr, T., Kappler, S. and Stierstorfer, K., "Polychromatic iterative statistical material image reconstruction for photon-counting computed tomography," Int. J. Biomed. Imag. 2016, 5871604 (2016).
[17] Alvarez, R.E. and Macovski, A., "Energy-selective reconstructions in X-ray computerised tomography," Phys. Med. Biol. 21(5), 733-744 (1976).
[18] Schirra, C.O., Roessl, E., Koehler, T., Brendel, B., Thran, A., Pan, D., Anastasio, M.A. and Proksa, R., "Statistical reconstruction of material decomposed data in spectral CT," IEEE Trans. Med. Imaging 32(7), 1249-1257 (2013).
[19] Clark, D.P. and Badea, C.T., "Spectral diffusion: an algorithm for robust material decomposition of spectral CT data," Phys. Med. Biol. 59(21), 6445-6466 (2014).
[20] Deuerling, J.M., Rudy, D. J.,. Niebur, G.L and Roeder, R.K., "Improved accuracy of cortical bone mineralization measured by polychromatic microcomputed tomography using a novel high mineral density composite calibration phantom," Med. Phys. 37(9), 5138-5145 (2010).
[21] Cole, L.E., Ross, R.D., Tilley, J.M.R., Vargo-Gogola, T. and Roeder, R.K., "Gold nanoparticles as contrast agents in X-ray imaging and computed tomography," Nanomedicine 10(2), 321-341 (2015).
[22] Berger, M., Hubbell, J., Seltzer, S., Chang, J., Coursey, J., Sukumar, R., Zucker, D. and Olsen, K., "XCOM: Photon cross section database (version 1.5)," National Institute of Standards and Technology, Gaithersburg, MD (2010). Available at http://physics.nist.gov/xcom.
[23] Themelis, K. and Rontogiannis, A.A., "A soft constrained MAP estimator for supervised hyperspectral signal unmixing," 16th European Signal Processing Conference (EUSIPCO), Lausanne, Switzerland (2008).